

Drude weight anisotropy in the doped iron pnictides: the primary role of orbital weight redistribution along the reconstructed Fermi surfaces

Dheeraj Kumar Singh^{1,2,3} and Pinaki Majumdar³

¹Department of Physics, POSTECH, Pohang, Gyeongbuk 790-784, Korea

²Asia Pacific Center for Theoretical Physics, Pohang, Gyeongbuk 790-784, Korea and

³Harish-Chandra Research Institute, HBNI, Chhatnag Road, Jhansi, Allahabad 211019, India

(Dated: April 21, 2022)

We explore the anisotropy in low frequency conductivity as a function of hole doping in multiorbital models of pnictides by analyzing the Drude weight in the x and y directions of a $(\pi, 0)$ spin-density wave state. A reduction in the conductivity anisotropy with increased hole doping, and subsequent sign reversal, both observed in experiments, is found to be a common trend in these models. This behavior arises due to the interplay of low energy orbitally-resolved density of states and the geometrical features of the Fermi surface. An understanding of anisotropy in the electron doped regime, however, would require additional ingredients.

PACS numbers: 74.70.Xa, 74.25.F-

I. INTRODUCTION

The anisotropic electronic properties of the iron pnictides, in both the collinear spin-density wave (SDW) state and the nematic state, have attracted considerable attention. Evidence of anisotropy is visible in angle-resolved photoemission spectroscopy^{1,2} (ARPES), nuclear magnetic resonance³ (NMR), scanning tunneling microscopy⁴, and transport measurements⁵⁻⁷. According to the ARPES measurements, a significant energy splitting between d_{xz} and d_{yz} orbitals is observed below the tetragonal-to-orthorhombic transition, which may either precede⁸ the SDW transition or occur simultaneously⁹, and states at the Fermi level have dominantly d_{xz} character¹⁰. In-plane anisotropy is observed also in the optical spectra¹¹ up to a photonic energy of 2eV.

The easiest to measure is transport anisotropy. Detwinned crystals show larger conductivity, surprisingly, in the antiferromagnetic direction compared to the ferromagnetic direction^{5,6,12}. The ratio of resistivities can be as large as 1.5 in the undoped parent compound. Similar conductivity anisotropy has also been observed in the nematic state^{7,12}.

Theories have tried to address the anisotropy. In the collinear SDW state of the undoped compound multiorbital models have been studied employing (i) a combination¹³ of the local density approximation (LDA) and dynamical mean field theory (DMFT), as well as (ii) mean-field methods¹⁴⁻¹⁶. According to these studies, a significant difference in the density of states (DOS) of d_{xz} and d_{yz} orbitals at the Fermi level may be responsible for the counter-intuitive anisotropy in the conductivity. Suppression of the DOS of d_{yz} orbital¹⁷ at the Fermi level, compared to that of d_{xz} , in the $(\pi, 0)$ -SDW state results in a larger conductivity along the x -direction since a major contribution to the Drude weight comes from the interorbital d_{xz} to d_{xy} hopping¹⁵. Conductivity in the y -direction, facilitated primarily by hopping between d_{yz} and d_{xy} , is smaller. Another study¹⁶ emphasizes the role of Fermi surface ‘reconstruction’. What about doped systems?

Experiments reveal that the conductivity anisotropy decreases and changes sign as hole doping increases⁷ while it grows on electron doping^{5,12}. In order to describe the doping dependence the role of doping induced disorder has been

invoked. It was shown that disorder with isotropic impurity potential can lead to elongated magnetic droplets in the nematic state, with anisotropy increasing as one approaches the SDW transition¹⁹⁻²². Deep inside the SDW state, the disorder has been suggested to be important particularly close to zero doping, where the Dirac point is situated near the Fermi level²³.

The role of both magnetic and non-magnetic disorder has indeed been explored experimentally. In the tetragonal state subjected to external strain, electron-doped samples having different residual resistivity show similar resistivity anisotropies²⁴. Studies on electron- and hole-doped samples, and the presence of magnetic impurities, drew a similar conclusion. This suggests that while disorder controls the magnitude of the resistivity, the anisotropy is more a consequence of the bandstructure in the doped system²⁵.

To conclusively settle this issue, we examined the Drude weight both in (a) the $(\pi, 0)$ -SDW state of the three-orbital model proposed by Daghofer *et al.*²⁶ and (b) the more sophisticated five-orbital models of Graser *et al.*²⁷ and Ikeda *et al.*²⁸. We find the following: (i) Despite considerable differences all these models exhibit the robust common feature that conductivity anisotropy decreases with hole doping, and subsequently reverses its sign - all consistent with experiments. (ii) We explain this in terms of the orbitally resolved weight along the Fermi surface, the hopping anisotropy, and shape of the Fermi surface. (iii) In the electron-doped region, the ratio of Drude weights along ferromagnetic and antiferromagnetic direction approaches ~ 1 asymptotically. Thus, experimental trend observed on electron doping is not captured within this approach, suggesting additional effects at play.

II. THEORY

We consider a multiorbital model Hamiltonian with the kinetic part defined as

$$\mathcal{H}_0 = - \sum_{i,j} \sum_{\mu,\nu,\sigma} t_{ij}^{\mu\nu} d_{i\mu\sigma}^\dagger d_{j\nu\sigma} \quad (1)$$

where the operator $d_{i\mu\sigma}^\dagger$ ($d_{i\mu\sigma}$) creates (destroys) an electron in the μ -th orbital of site \mathbf{i} with spin σ , and $t_{ij}^{\mu\nu}$ are the hopping elements from orbital μ and ν of sites \mathbf{i} and \mathbf{j} , respectively. The orbitals μ and ν belong to the set of five d -orbitals d_{xz} , d_{yz} , d_{xy} , $d_{x^2-y^2}$, and $d_{3z^2-r^2}$ depending on the model.

The interaction part of the Hamiltonian is given by

$$\mathcal{H}_{int} = U \sum_{\mathbf{i}, \mu} n_{i\mu\uparrow} n_{i\mu\downarrow} + (U' - \frac{J}{2}) \sum_{\mathbf{i}, \mu < \nu, \sigma \sigma'} n_{i\mu\sigma} n_{i\nu\sigma'} - 2J \sum_{\mathbf{i}} \mathbf{S}_{i\mu} \cdot \mathbf{S}_{i\nu} + J \sum_{\mathbf{i}, \sigma} d_{i\mu\sigma}^\dagger d_{i\mu\bar{\sigma}}^\dagger d_{i\nu\bar{\sigma}} d_{i\nu\sigma}$$

which includes the intraorbital (interorbital) Coulomb interaction term as the first (second) term. The third term describes the Hunds coupling, and the fourth term represents the pair hopping energy. Rotation-invariant interaction is ensured provided that $U' = U - 2J$.

The Hamiltonian after mean-field decoupling of the interaction term in the $(\pi, 0)$ -SDW state is given in the two sublattice basis by

$$\mathcal{H}_{mf} = \sum_{\mathbf{k}\sigma} \Psi_{\mathbf{k}\sigma}^\dagger (T_{\mathbf{k}\sigma} + M_{\mathbf{k}\sigma}) \Psi_{\mathbf{k}\sigma}, \quad (2)$$

where matrix elements $T_{\mathbf{k}\sigma}^{ll'}$ and $M_{\mathbf{k}\sigma}^{ll'} = -s\sigma\Delta_{l'}\delta^{ll'} + \frac{5J-U}{2}n_{l'}\delta^{ll'}$ are due to the kinetic and interaction parts, respectively. $l, l' \in s \otimes \mu$ with s and μ denoting a sublattice and an orbital, respectively. s and σ in front of $\Delta_{l'}\delta^{ll'}$ take value 1 (-1) for A (B) sublattice and \uparrow -spin (\downarrow -spin), respectively. The electron field operator and the exchange fields are defined as $\Psi_{\mathbf{k}}^\dagger = (d_{A\mathbf{k}1\uparrow}^\dagger, d_{A\mathbf{k}2\uparrow}^\dagger, \dots, d_{B\mathbf{k}1\uparrow}^\dagger, d_{B\mathbf{k}2\uparrow}^\dagger, \dots)$ and $2\Delta_l = Um_l + J \sum_{l' \neq l} m_{l'}$, respectively. Charge density n_l and magnetization m_l in each of the orbitals are determined self-consistently by diagonalizing the Hamiltonian.

The optical conductivity along $\alpha = x, y$ given by^{29,30}

$$\sigma_\alpha = D_\alpha \delta(\omega) + \frac{1}{N} \sum_{\mathbf{k}, n \neq n'} \frac{|j_{nn'}^\alpha(\mathbf{k})|^2}{E_{n'\mathbf{k}} - E_{n\mathbf{k}}} \times \theta(-E_{n'\mathbf{k}})\theta(E_{n\mathbf{k}})\delta(\omega - E_{n'\mathbf{k}} + E_{n\mathbf{k}}) \quad (3)$$

with Drude weight

$$\frac{D_\alpha}{2\pi} = \frac{1}{2N} \sum_{\mathbf{k}} T_{nn}^\alpha(\mathbf{k})\theta(-E_{n\mathbf{k}}) - \frac{1}{N} \sum_{\mathbf{k}, n \neq n'} \frac{|j_{nn'}^\alpha(\mathbf{k})|^2}{E_{n'\mathbf{k}} - E_{n\mathbf{k}}} \times \theta(-E_{n'\mathbf{k}})\theta(E_{n\mathbf{k}}). \quad (4)$$

θ is the step function, $E_{n\mathbf{k}}$ is the single particle energy in the ordered state with n as a band index, and

$$T_{nn}^\alpha = \sum_{\mu\nu} T_{nn}^{\alpha;\mu\nu} = \sum_{\mu\nu} \frac{\partial^2 t_{\mu\nu}(\mathbf{k})}{\partial k_x^2} a_{\mathbf{k}\mu n}^* a_{\mathbf{k}\nu n} \\ j_{nn'}^\alpha = - \sum_{\mu\nu} j_{nn'}^{\alpha;\mu\nu} = - \sum_{\mu\nu} \frac{\partial t_{\mu\nu}(\mathbf{k})}{\partial k_x} a_{\mathbf{k}\mu n}^* a_{\mathbf{k}\nu n'}, \quad (5)$$

$a_{\mathbf{k}\mu n}$ is the unitary matrix element between the orbital μ and band n in $(\pi, 0)$ -SDW state. To investigate the role of electronic reconstruction in the conductivity anisotropy, electron

scattering by impurities or spin fluctuations can be assumed to be isotropic for simplicity, which may not be the case in actuality³¹. However, absence of anisotropy due to impurity scattering is also supported by experiments. Then, δ function is approximated by Lorentzian with a small but non vanishing broadening parameter, which is same in both directions.

In this work we focus on the anisotropy in $\omega \rightarrow 0$ limit. To gain a better understanding of the origin of anisotropy, it is useful to define the components of Drude weight as¹⁵

$$\frac{D_l^{\alpha\beta}}{2\pi} = \frac{1}{2N} \sum_{\mathbf{k}} T_{nn}^{l;\alpha\beta}(\mathbf{k})\theta(-E_{n\mathbf{k}}) - \frac{1}{N} \sum_{\mathbf{k}, n \neq n'} \text{Re} \frac{j_{nn'}^{x(y);\alpha\beta^*}(\mathbf{k}) j_{nn'}^{x(y)}(\mathbf{k})}{E_{n'\mathbf{k}} - E_{n\mathbf{k}}} \theta(-E_{n'\mathbf{k}})\theta(E_{n\mathbf{k}}). \quad (6)$$

In the following, Hund's coupling J is set to be $U/4$ unless stated otherwise³², whereas intraorbital Coulomb interaction is chosen so that the total magnetic moment per site is nearly unity for the undoped case.

III. RESULTS

A. Three band model

Fig. 1(a) and (b) show the mean-field magnetic order parameter and the charge density of each of the orbitals in the $(\pi, 0)$ -SDW state for $U = 1.22\text{eV}$. Total magnetic moment increases continuously on moving from the electron- to hole-overdoped region. The difference in magnetization $m_{xz} - m_{yz}$ of two orbitals d_{xz} and d_{yz} reverses its sign slightly below

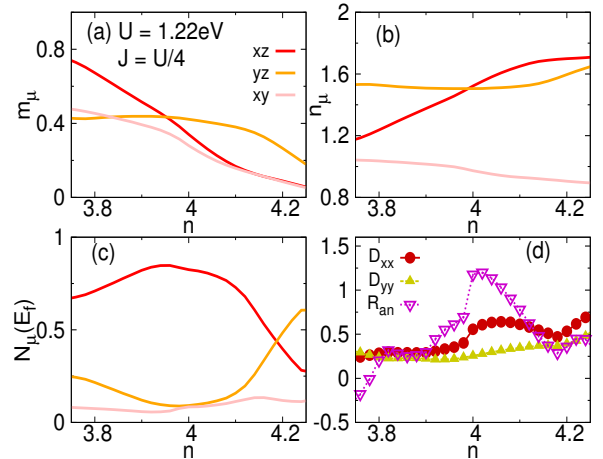


FIG. 1. Doping dependence of the (a) magnetic moment, (b) electronic density, and (c) DOS at the Fermi level for each of the orbitals in the $(\pi, 0)$ -SDW state of the three-orbital model of Daghofer *et al.* (d) Drude weights D_x and D_y in the x -direction and y -direction, respectively. For convenience, the dimensionless quantity $R_{an} = D_x/D_y - 1$, which provides a measure of the anisotropy, is also plotted.

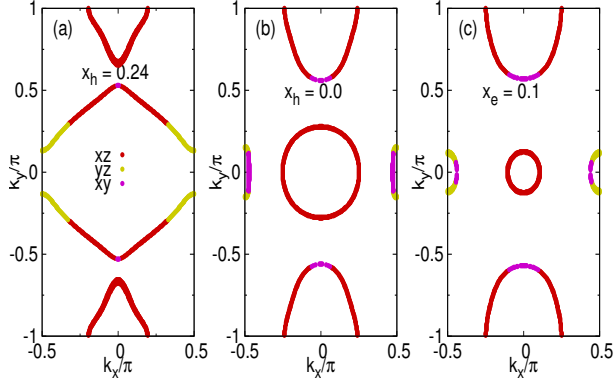


FIG. 2. Fermi surfaces in the $(\pi, 0)$ -SDW state of the model of Daghofer *et al.* for hole dopings (a) $x_h = 0.24$, (b) $x_h = 0.0$, and electron doping (c) $x_e = 0.1$ with the predominant orbital densities, where $U = 1.22\text{eV}$.

band-filling $n = 4.0$ which corresponds to the undoped case. A similar but opposite trend is observed for the ferro-orbital order $n_{xz} - n_{yz}$. As can also be seen from Fig. 1(d), sign reversal of the orbital order is not related to the reversal of anisotropy $R_{an} = D_x/D_y - 1$, where D_x and D_y are Drude weights along x - and y -directions, respectively. Latter occurs near hole doping $x_h \approx 0.22$ in agreement with the experiments. Note that SDW state for $x_h \approx 0.22$ may be stabilized only at higher temperature³³. R_{an} exhibits a maximum near zero doping and it's behavior in the electron doped region where it decreases is in contrast with the experiments.

Note that d_{xz} DOS remains dominant at the Fermi level for the entire hole-doping regime as shown in Fig. 1(c). Thus, suppression of d_{yz} DOS at Fermi level alone is not sufficient to explain the sign reversal. Apart from d_{xz} , d_{xy} orbital also plays a very important role in the anisotropy. As seen from Table I, interorbital D^{13} and intraorbital D^{33} contributions to the Drude weight are significant since the intraorbital hopping parameters t_{13} and t_{33} are considerably larger than t_{11} or t_{22} , where superscript 1, 2, and 3 have been used for the orbitals d_{xz} , d_{yz} , and d_{xy} , respectively. D_x^{13} remains larger than D_y^{13} despite a reduction in its value for the entire hole doping regime considered. At the same time, D_y^{33} becomes larger than D_x^{33} and contributes, apart from small contributions from D_y^{11} and D_y^{22} , substantially to the sign-reversal.

To understand the doping dependence it is essential to take into account the orbital-resolved DOS across the Fermi surface as well as the geometrical structure of the Fermi surfaces. Reconstruction of the hole pocket^{26,34-36} around Γ is not seen (Fig. 2(b)) which is in contrast with the experiments. This happens primarily because of larger interaction parameters chosen to yield magnetic moment $m_{tot} \approx 1$. However, reconstruction of the hole pockets for same magnetization can be clearly seen in the five-orbital model as presented below, which can disappear again on increasing the interaction³⁷.

The contribution to $D_{x(y)}^{13}$ comes from those regions of the Fermi surfaces, which have significant proportions of both

TABLE I. Components of Drude weight in the three orbital model for $U = 1.22\text{eV}$. α and β are orbital indices having values 1, 2, and 3 corresponding to the d_{xz} , d_{yz} , and d_{xy} orbitals, respectively. Subscripts 1, 2 and 3 of the components correspond to $x_h = 0.0$, $x_h = 0.24$ and $x_e = 0.1$ respectively.

$\alpha\beta$	11	12	13	22	23	33
$D_{x;1}^{\alpha\beta}$	0.010	0.000	0.098	-0.001	0.006	0.067
$D_{y;1}^{\alpha\beta}$	0.016	0.000	-0.010	0.001	0.007	0.070
$D_{x;2}^{\alpha\beta}$	0.002	0.000	0.045	0.000	0.017	0.017
$D_{y;2}^{\alpha\beta}$	0.011	0.000	0.019	0.012	0.012	0.041
$D_{x;3}^{\alpha\beta}$	0.002	0.001	0.117	-0.001	0.006	0.074
$D_{y;3}^{\alpha\beta}$	0.009	0.000	-0.014	0.002	0.012	0.104

the orbitals d_{xz} and d_{yz} . In the undoped case, such regions are near $(\pm 0.24\pi, \pm\pi)$ of the electron pockets at $(0, \pm\pi)$ and also near the boundary separating d_{yz} and d_{xy} dominated regions of the hole pockets at $(0, \pm 0.5\pi)$ (Fig.2(b)). Moreover, components of the Fermi velocity along those regions follow the relation $v_x^f > v_y^f$. For this reason, D_x^{13} is significantly larger than D_y^{13} , and thus primarily responsible for the Drude weight anisotropy. Other important contributor $D_{x(y)}^{33}$ do not differ substantially in the x - and y -directions for zero doping. This is because nearly equal regions of the electron pocket at $(0, \pm\pi)$ and the hole pockets at $(\pm 0.5\pi, 0)$ dominated by the d_{xy} orbital have Fermi velocity components mainly along y - and x -direction, respectively. The hole pocket around $(0, 0)$ is nearly circular and predominantly of d_{xz} character, thus does not contribute to the anisotropy.

On electron doping, d_{xy} dominated sections of the electron pockets and hole pockets get shrunk and enlarged, respectively, (Fig. 2(c)). This leads to $D_y^{33} > D_x^{33}$ causing a drop in R_{an} . Whereas contribution due to $D_{(x)y}^{13}$ becomes smaller

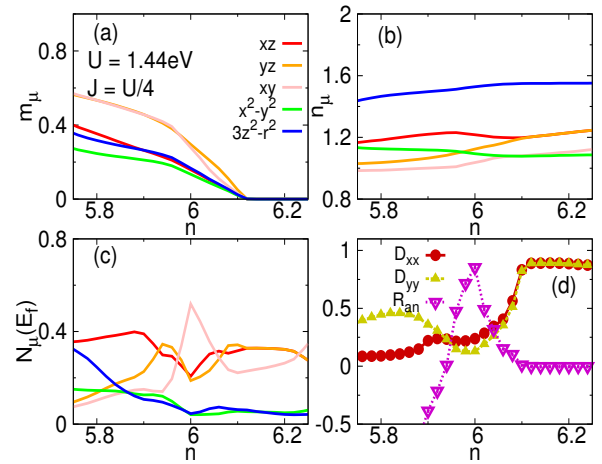


FIG. 3. (a) Orbital magnetizations (b) orbital densities (c) orbital resolved DOS at the Fermi level as a function of doping in the five-orbital model of Graser *et al.* (d) Drude weight in the x -direction, y -direction, and the anisotropy.

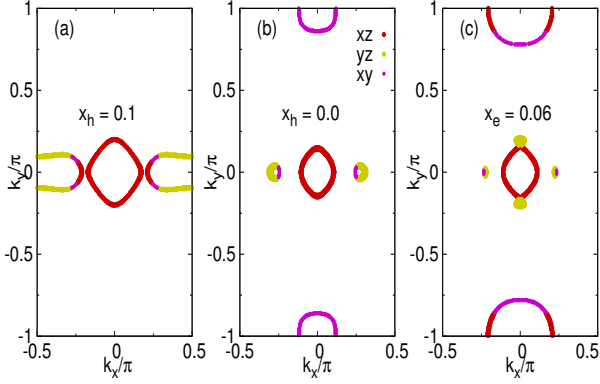


FIG. 4. Fermi surfaces for hole dopings (a) $x_h = 0.1$, (b) $x_h = 0.0$, and electron doping (c) $x_e = 0.06$ with dominant orbital character in the model of Graser *et. al.*, where $U = 1.44\text{eV}$.

(Fig. 2(a)) on hole doping. Finally, the regions of square-like Fermi surface with dominant d_{xz} and d_{xy} orbitals have $v_x^f > v_y^f$ in large region leading to $D_y^{33} > D_x^{33}$, which results in the reversal of Drude-weight anisotropy.

B. Five band model of Graser *et al.*

In the five-orbital model of Graser *et. al.*, orbital magnetization shows a quick rise on hole doping so that $\sum_\mu m_\mu \geq 1.6$ as soon as doping reaches 0.1, while it decreases rapidly on electron doping and vanishes near $n \approx 6.12$ (Fig. 3(a)). $n \approx 6.0$ corresponds to the undoped case $x = 0$. There is a significant difference in the magnetizations as well as in the charge densities of d_{xz} and d_{yz} orbitals. The ferro-orbital order $n_{xz} - n_{yz}$ has a sign opposite to that of $m_{xz} - m_{yz}$ in the entire region of electron density considered here (Fig. 3(b)). Unlike the three-orbital model, there is no sign reversal of these parameters.

Before discussing the Drude weight anisotropy in this model, it is interesting to look first at the orbitally-resolved relative DOS at the Fermi level. As seen from Fig. 3(c), the DOS of d_{xy} orbital is the largest for the undoped case in contrast with the three-orbital model, which decreases upon doping either holes or electrons. On the other hand, DOSs of d_{xz} and d_{yz} orbitals, though small and nearly equal for zero doping, increase on doping either electrons or holes.

R_{an} is maximum near $x_h \approx 0$, drops rapidly, and changes sign near $x_h \approx 0.07$ (Fig. 3(d)). This drop is significantly faster in comparison with the three-orbital model. Another important difference from the previous model is that the Drude weight is larger in the x -direction despite DOSs of d_{xz} and d_{yz} orbitals being nearly equal at the Fermi level in the undoped case. Although the same component D^{14} is responsible for this anisotropy (superscript 4 here refers to d_{xy} orbital, Table II), which implies again a crucial role of the orbitally-resolved DOS distribution along the Fermi surfaces. The sections of the Fermi surfaces having significant proportions of both d_{xz} and d_{xy} orbitals are near $(\pm 0.12\pi, \pm\pi)$ of the electron pocket-

TABLE II. Elements of Drude weight in the model of Graser *et. al.* for $U = 1.44\text{eV}$. Here, orbital indices having values 1, 2, 3, 4, and 5, which correspond to the d_{xz} , d_{yz} , $d_{x^2-y^2}$, d_{xy} , and $d_{3z^2-r^2}$ orbitals, respectively. Subscripts 1, 2 and 3 correspond to $x_h = 0.0$, $x_h = 0.1$ and $x_e = 0.06$, respectively

$\alpha\beta$	11	14	23	24	35	44	45
$D_{x:1}^{\alpha\beta}$	0.017	0.037	0.002	0.000	-0.001	0.019	0.000
$D_{y:1}^{\alpha\beta}$	0.010	0.000	0.001	0.004	0.000	0.017	0.000
$D_{x:2}^{\alpha\beta}$	0.016	0.035	0.000	0.000	0.000	0.024	0.000
$D_{y:2}^{\alpha\beta}$	0.010	-0.001	0.021	0.043	0.008	0.003	0.019
$D_{x:3}^{\alpha\beta}$	0.030	0.085	-0.002	0.000	0.000	0.010	0.000
$D_{y:3}^{\alpha\beta}$	0.007	0.003	0.000	0.021	0.000	0.069	0.000

ets at $(0, \pm\pi)$ and are also near the d_{xy} dominated regions of the small hole pockets at $(\pm 0.27\pi, 0)$ (Fig. 4(b)). Moreover, $v_x^f > v_y^f$ in these regions, which is mainly responsible for the anisotropy. Like the three-orbital model, the hole pocket at $(0, 0)$ is predominantly of d_{xz} orbital character ($\approx 88\%$), thus does not play an important role in the anisotropy.

The electron pocket grows with a significant modification in the orbitally-resolved DOS distribution on electron doping in such a way that D_x^{14} increases further while D_y^{14} remains vanishingly small (Fig. 4(c)). This is because the regions of the pocket with nearly equal proportions of both d_{xz} and d_{xy} orbitals have $v_x^f > v_y^f$. However, D_y^{44} becomes significantly larger than D_x^{44} (table II) as d_{xy} orbital dominates now only those sections which have $v_x^f < v_y^f$. For this reason, there is a net decline in R_{an} .

On the other hand, the electron pocket becomes smaller and disappear on hole doping $x_h \approx 0.1$. Meanwhile, the hole pockets at $(\pm 0.27\pi, 0)$ grows larger in size until they get connected to the hole pocket at $(0, 0)$ and also extended in the opposite direction (Fig. 4(a)). As seen from table II, anisotropy in D^{14} remains largely unaffected because of the regions of

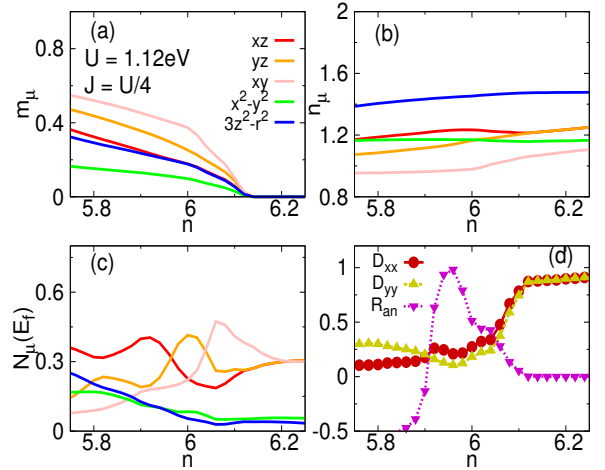


FIG. 5. (a) Magnetization, (b) charge density (c) DOS at the Fermi level for each of the orbitals. (d) Drude weights in x - and y -directions, and their ratios in the model of Ikeda *et. al.*

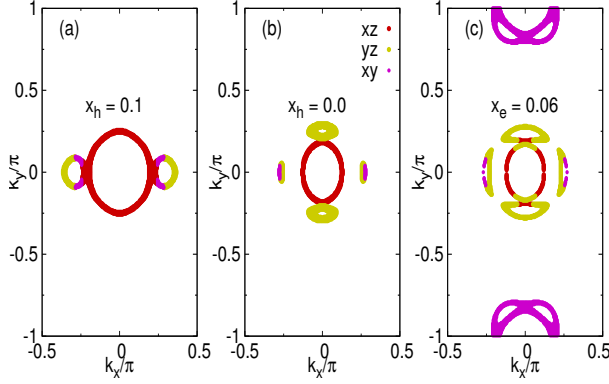


FIG. 6. Fermi surfaces for hole dopings (a) $x_h = 0.1$, (b) $x_h = 0.0$, and (c) $x_e = 0.06$ with color showing leading orbital character in the five-orbital model of Ikeda *et. al.*, where $U = 1.12\text{eV}$.

hole pockets having $v_x^f > v_y^f$ significant proportions of d_{xz} and d_{xy} orbitals. Whereas the flat regions of the hole pocket with $v_y^f > v_x^f$ (vanishingly small v_x^f) have significant proportions of d_{yz} as well as of either d_{xy} or $d_{x^2-y^2}$ orbitals, which leads to $D_y^{23} > D_x^{23}$ and $D_y^{24} > D_x^{24}$ (Table II), hence leading to the sign reversal of R_{an} .

C. Five band model of Ikeda *et. al.*

The doping dependence of magnetic moment and charge density of each of the orbitals is similar to that of the model of Graser *et. al.* (Fig. 5(a) and (b)). However, the DOS of d_{yz} orbital is largest at the Fermi level in the undoped case in contrast with the previously discussed two models (Fig. 5(c)). Behavior of R_{an} as a function of hole doping is more or less similar to the model of Graser *et. al.* except that the peak and zero of the anisotropy are shifted towards a point near $x_h \approx 0.04$ and $x_h \approx 0.09$, respectively (Fig. 5(d)). Another significant difference from the previous model is the absence of the electron pocket around $(0, \pm\pi)$ for zero doping.

The leading source of anisotropy for the undoped case is

TABLE III. Elements of Drude weight in the model of Ikeda *et. al.* for $U = 1.12\text{ eV}$. Here, orbital indices having values 1, 2, 3, 4, and 5, which correspond to the d_{xz} , d_{yz} , $d_{x^2-y^2}$, d_{xy} , and $d_{3z^2-r^2}$ orbitals, respectively. Subscripts 1, 2 and 3 correspond to $x_h = 0.0$, $x_h = 0.1$ and $x_e = 0.06$, respectively

$\alpha\beta$	11	14	23	24	35	44	45
$D_{x;1}^{\alpha\beta}$	0.026	0.038	-0.002	0.000	-0.001	0.010	0.000
$D_{y;1}^{\alpha\beta}$	0.012	-0.001	0.000	0.014	0.005	0.000	0.000
$D_{x;2}^{\alpha\beta}$	0.027	0.021	0.002	0.000	-0.004	0.006	-0.002
$D_{y;2}^{\alpha\beta}$	0.013	-0.001	0.003	0.024	0.011	0.001	0.006
$D_{x;3}^{\alpha\beta}$	0.025	0.057	0.003	0.001	0.002	0.034	-0.001
$D_{y;3}^{\alpha\beta}$	0.013	0.001	0.000	0.032	0.005	0.024	0.000

$D_x^{14} > D_y^{14}$, which originates mainly from the small electron pockets near $(\pm 0.25\pi, 0)$, which are extended along y -direction. The reason is similar to that described in the previous model in terms of the orbitally-resolved DOS distributions (Fig. 6(b)). The anisotropy vanishes close to $x_h \approx 0.1$ because of the hole pockets being nearly circular (Fig. 6(b)). Major components contributing to the Drude weight within the range $0 \lesssim x_h \lesssim 0.1$ remains similar to that within the model of Graser *et. al.* Moreover, their behavior as a function of doping is also similar. But there are important differences in the electron-doped region. Here, the suppression of anisotropy does not result from a large anisotropy in the D^{44} component ($D_y^{44} \gg D_x^{44}$). In fact, D_x^{44} remains greater than D_y^{44} largely because of the difference in orbital-weight distribution along the electron pocket near $(\pm\pi, 0)$. Thus, unlike D^{44} , D^{24} is mainly responsible for the reduction in anisotropy on electron doping.

D. Anisotropy in the nematic phase

In order to understand the conductivity anisotropy in the nematic phase, which is found to be significant $\sigma_a/\sigma_b \sim 1.2$ in the transport measurements, we consider an explicit orbital-splitting term as observed by the ARPES measurements in addition to the kinetic part of the Hamiltonian (Eq. (1))

$$\mathcal{H}_{OO} = \frac{\delta}{2} \sum_i (d_{iyz\sigma}^\dagger d_{iyz\sigma} - d_{ixz\sigma}^\dagger d_{ixz\sigma}). \quad (7)$$

Consideration of the term has limited motivation that is to focus on it's impact on the anisotropy instead of it's origin. Recent works trace the origin to many-body effects beyond the random-phase approximation level³⁸. Furthermore, an alternative scenario of conductivity anisotropy, where electrons gets scattered by the critical-spin fluctuations, has also been proposed³⁹.

Table IV, V and VI show relevant components of Drude weight obtained for $\delta = 80\text{meV}$ in the undoped case. Interestingly, we find anisotropy in all the three models to be arising due to the anisotropy in the interorbital component of Drude weight corresponding to the d_{xy} orbital indicating that the orbital splitting affects orbital distribution of d_{xy} the most along the Fermi surfaces. Anisotropy is significant $\sim 8\%$ ($D_y > D_x$) in each model but smaller against experimentally observed $\sim 20\%$. Thus, orbital splitting induced redistribution of d_{xy} orbital may contribute significantly to the conductivity anisotropy in the nematic phase.

TABLE IV. Components of Drude weight in the model of Daghofer *et. al.* for $\delta = 80\text{meV}$. α and β are orbital indices having values 1, 2, and 3 corresponding to the d_{xz} , d_{yz} , and d_{xy} orbitals, respectively.

$\alpha\beta$	11	12	13	22	23	33
$D_x^{\alpha\beta}$	0.008	0.000	0.136	0.029	-0.003	0.099
$D_y^{\alpha\beta}$	0.013	-0.001	-0.010	0.034	0.135	0.121

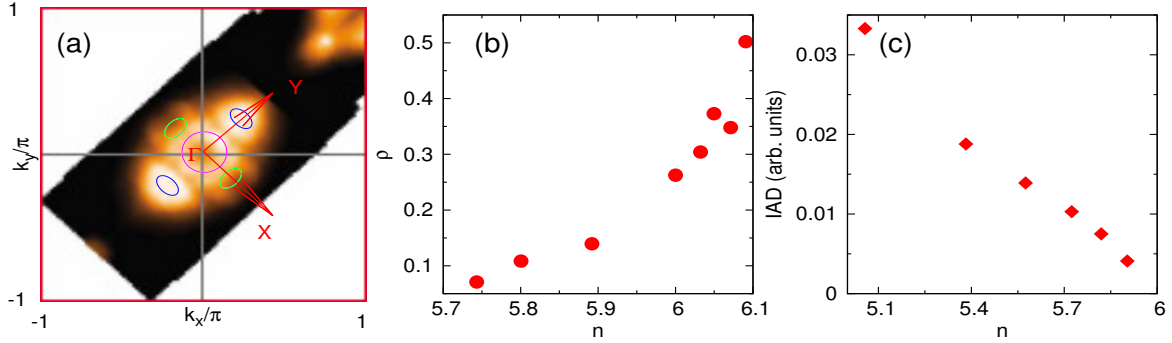


FIG. 7. (a) ARPES Fermi surfaces obtained for 3.5% electron-doped CaFe_2As_2 in the orthorhombic state with collinear magnetic order. k_x and k_y are the reciprocal lattice vectors defined corresponding to the unit cell consisting of two Fe atoms (Ref. [34]). High symmetry directions in the SDW state are rotated by 45° . (b) Resistivity anisotropy $\rho = \rho_b/\rho_a - 1$ in BaFe_2As_2 at $0.95T_N$ reproduced from Ref. [7], where b and a are the ferromagnetic and the antiferromagnetic axes, respectively. (c) Integrated absolute difference (IAD) from X-ray emission spectroscopy as a function of hole doping for BaFe_2As_2 , which provides a qualitative estimate of the behavior of local moments as a function of hole doping (Ref. [41]).

TABLE V. Elements of Drude weight in the model of Graser *et. al.* for $\delta = 80\text{meV}$. Here, orbital indices having values 1, 2, 3, 4, and 5, which correspond to the d_{xz} , d_{yz} , $d_{x^2-y^2}$, d_{xy} , and $d_{3z^2-r^2}$ orbitals, respectively.

$\alpha\beta$	11	22	33	44	55	13	14
$D_x^{\alpha\beta}$	0.043	0.024	0.001	0.063	0.000	0.007	0.100
$D_y^{\alpha\beta}$	0.023	0.045	0.002	0.080	0.000	0.026	0.004

TABLE VI. Elements of Drude weight in the model of Ikeda *et. al.* with parameters and conventions as in Table V.

$\alpha\beta$	11	22	33	44	55	13	14
$D_x^{\alpha\beta}$	0.050	0.020	0.004	0.071	0.000	0.007	0.096
$D_y^{\alpha\beta}$	0.020	0.050	0.005	0.092	0.000	0.033	0.004

IV. DISCUSSION

The ratio of the Drude weights along the antiferromagnetic and ferromagnetic directions drops from $D_x/D_y \sim 2$ to a lower value on moving away from $x \sim 0$. This compares well with $\sigma_x/\sigma_y \sim 1.5$ for $\omega \rightarrow 0$ and $x \sim 0$ in the optical conductivity measurement where it is found to be $\sim 1.5^{11}$. A similar value of conductivity ratio is obtained in the transport measurements highlighting the important role of band structure.

Despite the similarities exhibited by these models with respect to doping dependence of local moment and Drude weight anisotropy, several features of their Fermi surface are different. In the models of Daghofer *et. al.* and Graser *et. al.*, a very important role in the anisotropy is played by the electron pockets at $(0, \pm\pi)$, absent in the model of Ikeda *et. al.* ARPES measurements do find a weak signature of small electron pockets around X. However, most crucial features such as the electron pockets placed slightly away from Γ along Γ -X

and Γ -Y of the model of Ikeda *et. al.* are in very good agreement with the experiments except the ellipse-like hole pocket around Γ which may be either absent or whose signature may be very weak to be visible²². In other words, yellow electron pockets and the electron pocket with two different regions having different leading orbital character (Fig. 6(c)) show a good correspondence to the blue and the green electron pockets of experimental Fermi surfaces (Fig. 7(a)), respectively. Overall, a better agreement with the experiments regarding the Fermi-surface characteristics is exhibited within this model. It is also important to note that the electron pockets are mainly responsible for the anisotropy even in this model. Moreover, similar electron pockets occur also in the model of Graser *et. al.* though their role is not as significant as in the model of Ikeda *et. al.* because of their smaller sizes.

Drude weight anisotropy in all the three model explored here exhibit a common trend. Continuous decline and sign reversal on hole doping compares very well the experiments while the decline on electron doping is in contrast with the measurements⁷. The decrease of anisotropy on hole doping is not so fast in the three-orbital model owing largely to a slow modification in the electronic structure, whereas a sharp decline is exhibited in the five-orbital models.

Magnetic moment grows on moving from the electron-doped towards the hole-doped region irrespective of the models. This is not surprising because in each of the models, one approaches half filling on doping holes, which suppresses electron movement in the lattice leading to the departure from metallicity, and finally to the Mottness as also pointed out by a recent density functional theory (DFT) combined with slave-spin mean-field approach⁴⁰. Evidence in support of growing magnetic moment on hole doping has been substantiated recently by the X-ray emission spectroscopy using integrated absolute difference (IAD)⁴¹.

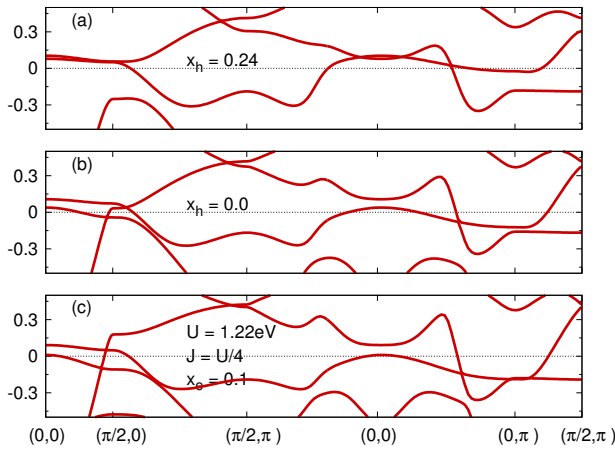


FIG. 8. Electronic dispersion in the $(\pi, 0)$ -SDW state along high-symmetry directions within the three-orbital model of Daghofer *et al.*

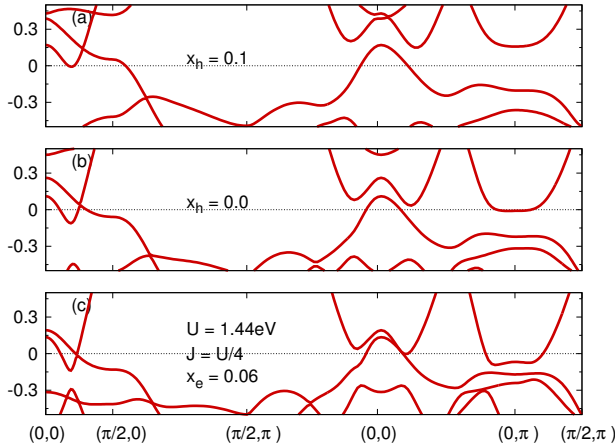


FIG. 9. Same as in Fig.8 but for the five-orbital model of Graser *et al.*

V. CONCLUSIONS

We have established the role of bandstructure on the doping dependence of conductivity anisotropy by examining the Drude weights within the widely used models of pnictides. In all of them, the anisotropy exhibits a maximum near zero doping, decreases on doping holes, and then reverses sign at a certain hole doping, all in qualitative agreement with the experiments. However, we also find that the anisotropy decreases on electron doping and vanishes, a feature in contrast with the experiments, clearly implying the role of other factors such as doping induced disorder.

We explain the origin of anisotropy and its doping dependence in terms of the topology and shape of the Fermi surfaces as well as the distribution of orbital-resolved DOS along them - not just the dominance of some particular DOS orbital at the Fermi level. This is reflected in the similar anisotropy behavior of different models despite the dominance of different low energy orbitals in them. The leading contributor to the anisotropy common for all the models is interorbital hopping processes involving d_{xz} and d_{xy} orbitals. In the nematic phase, a significant anisotropy is obtained due to the redistribution of orbital weight which affects d_{xy} orbital the most. Overall, the d_{xy} orbital plays the most crucial role in the conductivity anisotropy in the iron pnictides.

ACKNOWLEDGMENT

We acknowledge use of the HPC Clusters at HRI.

APPENDIX: ELECTRONIC DISPERSION IN THE $(\pi, 0)$ -SDW STATE

Electronic dispersions for the different models are presented for the parameters discussed above. Fig. 8 shows dispersion along high-symmetry directions for the dopings (a) $x_h = 0.24$, (b) $x_h = 0.0$, and (c) $x_e = 0.1$ in the three-orbital model of Daghofer *et al.* with $U = 1.22\text{eV}$. Fig. 9 shows dispersion for the dopings (a) $x_h = 0.1$, (b) $x_h = 0.0$, and (c) $x_e = 0.06$ in the five-orbital model of Graser *et al.* with $U = 1.44\text{eV}$. Fig. 10 shows dispersion for the dopings (a) $x_h = 0.1$, (b) $x_h = 0.0$, and (c) $x_e = 0.06$ in the five-orbital model of Ikeda *et al.* with $U = 1.12\text{eV}$.

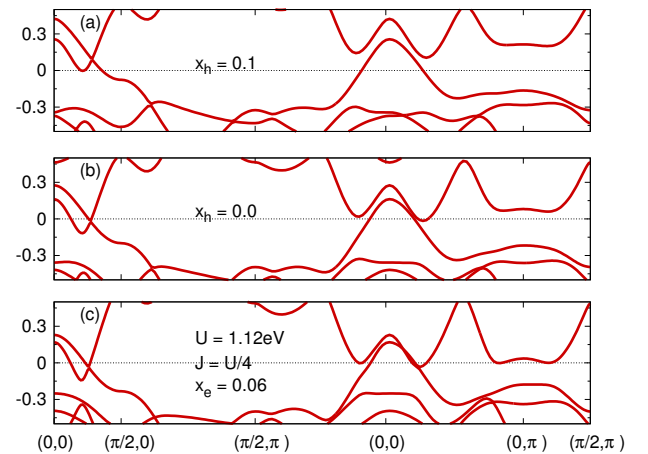


FIG. 10. Same as in Fig.9 but for the model of Ikeda *et al.*

¹ M. Yi, D. Lu, J.-H. Chu, J. G. Analytis, A. P. Sorini, A. F. Kemper, B. Moritz, S.-K. Mo, R. G. Moore, M. Hashimoto, W.-S. Lee, Z. Hussain, T. P. Devereaux, I. R. Fisher, and Z.-X. Shen, Proc. Natl.

Acad. Sci. **108**, 6878 (2011).

² T. Shimojima, T. Sonobe, W. Malaeb, K. Shinada, A. Chainani, S. Shin, T. Yoshida, S. Ideta, A. Fujimori, H. Kumigashira, K.

- Ono, Y. Nakashima, H. Anzai, M. Arita, A. Ino, H. Namatame, M. Taniguchi, M. Nakajima, S. Uchida, Y. Tomioka, T. Ito, K. Kihou, C. H. Lee, A. Iyo, H. Eisaki, K. Ohgushi, S. Kasahara, T. Terashima, H. Ikeda, T. Shibauchi, Y. Matsuda, and K. Ishizaka, *Phys. Rev. B* **89**, 045101 (2014).
- ³ M. Fu, D. A. Torchetti, T. Imai, F. L. Ning, J.-Q. Yan, and A. S. Sefat, *Phys. Rev. Lett.*, **109**, 247001 (2012).
- ⁴ T.-M. Chuang, M. P. Allan, J. Lee, Y. Xie, N. Ni, S. L. Budko, G. S. Boebinger, P. C. Canfield, and J. C. Davis, *Science* **327**, 181 (2010).
- ⁵ J.-H. Chu, J.-H. Chu, J. G. Analytis, K. De Greve, P. L. McMahon, Z. Islam, Y. Yamamoto, and I. R. Fisher, *Science* **329**, 824 (2010).
- ⁶ M. A. Tanatar, E. C. Blomberg, A. Kreyssig, M. G. Kim, N. Ni, A. Thaler, S. L. Bud'ko, P. C. Canfield, A. I. Goldman, I. I. Mazin, and R. Prozorov, *Phys. Rev. B* **81**, 184508 (2010).
- ⁷ E. C. Blomberg, M. A. Tanatar, R. M. Fernandes, I. I. Mazin, B. Shen, H.-H. Wen, M. D. Johannes, J. Schmalian, and R. Prozorov, *Nat. Commun.* **4**, 1914 (2013).
- ⁸ S. Nandi, M. G. Kim, A. Kreyssig, R. M. Fernandes, D. K. Pratt, A. Thaler, N. Ni, S. L. Budko, P. C. Canfield, J. Schmalian, R. J. McQueeney, and A. I. Goldman, *Phys. Rev. Lett.*, **104**, 057006 (2010).
- ⁹ M. Rotter, M. Tegel, D. Johrendt, I. Schellenberg, W. Hermes, and R. Pöttgen, *Phys. Rev. B*, **78**, 020503R (2008).
- ¹⁰ T. Shimojima, K. Ishizaka, Y. Ishida, N. Katayama, K. Ohgushi, T. Kiss, M. Okawa, T. Togashi, X.-Y. Wang, C.-T. Chen, S. Watanabe, R. Kadota, T. Oguchi, A. Chainani, and S. Shin, *Phys. Rev. Lett.* **104**, 057002 (2010).
- ¹¹ M. Nakajima, T. Liang, S. Ishida, Y. Tomioka, K. Kihou, C. H. Lee, A. Iyo, H. Eisaki, T. Kakeshita, T. Ito, and S. Uchida, *Proc. Natl. Acad. Sci. U.S.A.* **108**, 12238 (2011).
- ¹² J. J. Ying, X. F. Wang, T. Wu, Z. J. Xiang, R. H. Liu, Y. J. Yan, A. F. Wang, M. Zhang, G. J. Ye, P. Cheng, J. P. Hu, and X. H. Chen, *Phys. Rev. Lett.* **107**, 067001 (2011).
- ¹³ Z. P. Yin, K. Haule, and G. Kotliar, *Nat. Phys.* **7**, 294 (2011).
- ¹⁴ K. Sugimoto, E. Kaneshita, and T. Tohyama, *J. Phys. Soc. Jpn.* **80**, 033706 (2011).
- ¹⁵ X. Zhang and E. Dagotto, *Phys. Rev. B* **84**, 132505 (2011).
- ¹⁶ B. Valenzuela, E. Bascones, and M. J. Calderón, *Phys. Rev. Lett.* **105**, 207202 (2010).
- ¹⁷ M. Daghofer, Q.-L. Luo, R. Yu, D. X. Yao, A. Moreo, and E. Dagotto, *Phys. Rev. B* **81**, 180514(R) (2010).
- ¹⁸ S. Liang, G. Alvarez, C. Sen, A. Moreo, and E. Dagotto, *Phys. Rev. Lett.* **109**, 047001 (2012).
- ¹⁹ M. N. Gastiasoro, I. Paul, Y. Wang, P. J. Hirschfeld, and B. M. Andersen, *Phys. Rev. Lett.* **113**, 127001 (2014).
- ²⁰ M. Breitzkreiz, P. M. R. Brydon, and C. Timm, *Phys. Rev. B* **90**, 121104(R) (2014).
- ²¹ D. K. Singh and P. Majumdar, *Phys. Rev. B* **96**, 235111 (2017); D. K. Singh, A. Akbari, and P. Majumdar, arXiv:1805.09582
- ²² Y. Wang, Maria N. Gastiasoro, Brian M. Andersen, M. Tomic, H. O. Jeschke, R. Valent, I. Paul, and P. J. Hirschfeld, *Phys. Rev. Lett.* **114**, 097003 (2015).
- ²³ K. Sugimoto, P. Prelovšek, E. Kaneshita, and T. Tohyama, *Phys. Rev. B* **90**, 125157 (2014).
- ²⁴ H.-H. Kuo and I. R. Fisher, *Phys. Rev. Lett.* **112**, 227001 (2014).
- ²⁵ T. Kobayashi, K. Tanaka, S. Miyasaka, and S. Tajima, *J. Phys. Soc. Jpn.* **84**, 094707 (2015).
- ²⁶ M. Daghofer, A. Nicholson, A. Moreo, and E. Dagotto, *Phys. Rev. B* **81**, 014511 (2010).
- ²⁷ S. Graser, T. Maier, P. Hirschfeld, and D. Scalapino, *New J. Phys.* **11**, 025016 (2009).
- ²⁸ H. Ikeda, R. Arita, and J. Kunes, *Phys. Rev. B* **81**, 054502 (2010).
- ²⁹ E. Dagotto, *Rev. Mod. Phys.* **66**, 763 (1994).
- ³⁰ B. Valenzuela, M. J. Calderón, G. León, and E. Bascones, *Phys. Rev. B* **87**, 075136 (2013).
- ³¹ A. F. Kemper, M. M. Korshunov, T. P. Devereaux, J. N. Fry, H.-P. Cheng, and P. J. Hirschfeld, *Phys. Rev. B* **83**, 184516 (2011).
- ³² A. A. Schafgans, S. J. Moon, B. C. Pursley, A. D. LaForge, M. M. Qazilbash, A. S. Sefat, D. Mandrus, K. Haule, G. Kotliar, and D. N. Basov, *Phys. Rev. Lett.* **108**, 147002 (2012).
- ³³ S. Avci, O. Chmaissem, D. Y. Chung, S. Rosenkranz, E. A. Goremychkin, J. P. Castellán, I. S. Todorov, J. A. Schlueter, H. Claus, A. Daoud-Aladine, D. D. Khalyavin, M. G. Kanatzidis, and R. Osborn, *Phys. Rev. B* **85**, 184507 (2012).
- ³⁴ M. Yi, D. H. Lu, J. G. Analytis, J.-H. Chu, S.-K. Mo, R.-H. He, M. Hashimoto, R. G. Moore, I. I. Mazin, D. J. Singh, Z. Hussain, I. R. Fisher and Z.-X. Shen, *Phys. Rev. B* **80**, 174510 (2009).
- ³⁵ D. H. Lu, M. Yi, S.-K. Mo, J. G. Analytis, J.-H. Chu, A. S. Erickson, D. J. Singh, Z. Hussain, T. H. Geballe, I. R. Fisher, Z.-X. Shen, *Physica C* **469**, 452 (2009).
- ³⁶ C. Liu, T. Kondo, R. M. Fernandes, A. D. Palczewski, E. D. Mun, N. Ni, A. N. Thaler, A. Bostwick, E. Rotenberg, J. Schmalian, S. L. Budko, P. C. Canfield and A. Kaminski, *Nat. Phys.* **6**, 419 (2010).
- ³⁷ M. Kovacic, M. H. Christensen, M. N. Gastiasoro and B. M. Andersen, *Phys. Rev. B* **91**, 064424 (2015).
- ³⁸ S. Onari and H. Kontani, *Phys. Rev. B* **96**, 094527 (2017).
- ³⁹ R. M. Fernandes, E. Abrahams and J. Schmalian, *Phys. Rev. Lett* **107**, 217002 (2011).
- ⁴⁰ L. de' Medici, G. Giovannetti, and M. Capone, *Phys. Rev. Lett.* **112**, 177001 (2014).
- ⁴¹ S. Lafuerza, H. Gretarsson, F. Hardy, T. Wolf, C. Meingast, G. Giovannetti, M. Capone, A. S. Sefat, Y. -J. Kim, P. Glatzel, and L. de' Medici, *Phys. Rev. B* **96**, 045133 (2017).